AGU ADVANCING EARTH AND SPACE SCIENCES

JGR Space Physics

RESEARCH ARTICLE

10.1029/2025JA034390

Key Points:

- Daytime Equatorial Electrojet (EEJ) intensity tripled during the main storm phase and returned to normal levels during the recovery phase
- In the midnight sector eastward midlatitude and westward equatorial current jets correspond to enhanced or reversed dayside EEJ
- The enhancement of the daytime EEJ and the emergence of the nighttime EEJ are highly sensitive to the onset of geomagnetic storm

Correspondence to:

X. Xu and R. Shi,
xjxu@must.edu.mo;
20123@tongji.edu.cn

Citation:

Xiong, Y., Xu, X., Shi, R., Han, D., & Li, H. (2026). Macau Scientific Satellite-1 observations of the equatorial electrojets during the geomagnetic storm on May 10–13, 2024. *Journal of Geophysical Research: Space Physics*, *131*, e2025JA034390. https://doi.org/10.1029/2025JA034390

Received 6 SEP 2025
Accepted 15 APR 2026

Macau Scientific Satellite-1 Observations of the Equatorial Electrojets During the Geomagnetic Storm on May 10–13, 2024

Yating Xiong[1,2,3], Xiaojun Xu[4], Run Shi[5], Desheng Han[5], and Hui Li[2]

[1]State Key Laboratory of Environment Characteristics and Effects for Near-Space, Nanjing University of Information Science and Technology, Nanjing, China, [2]State Key Laboratory of Space Weather, Chinese Academy of Sciences, Beijing 100190, China, [3]Tiandu-Nuist Deep Space Exploration Laboratory, Nanjing University of Information Science and Technology, Nanjing, China, [4]State Key Laboratory of Lunar and Planetary Sciences, Macau University of Science and Technology, Macao 999078, China, [5]State Key Laboratory of Marine Geology, School of Ocean and Earth Science, Tongji University, Shanghai, China

Abstract The characteristics of the equatorial electrojet (EEJ) under extreme geomagnetic disturbance conditions, particularly on the nightside, have remained relatively unexplored. Utilizing high-precision magnetic field measurements from the MSS-1A satellite together with observations from the Swarm satellite, we investigate the EEJ during a super geomagnetic storm. The dayside EEJ evolution observed by Swarm B during the storm is highly consistent with that derived from MSS-1A observations. On the dayside, the eastward EEJ intensified after the storm onset and reached a peak at −20.8 nT near the magnetic equator, corresponding to a current density of 75.2 mA/m, during the initial and main phases. During the recovery phase, the EEJ stabilized at −8.3 nT (25 mA/m), resembling quiet-time climatology. On the nightside, westward current jets near the equator are observed during intense geomagnetic storm activity. Interestingly, strong eastward current jets also emerge at low to middle latitudes. These results demonstrate that the enhancement of the dayside EEJ and the appearance of the nightside EEJ are sensitive to storm onset. They also indicate that prompt penetration electric fields, disturbance dynamo electric fields, and overshielding electric fields play distinct roles during different phases of the geomagnetic storm.

Plain Language Summary The equatorial electrojet (EEJ) is a narrow, intense current that flows along the magnetic equator in the Earth's upper atmosphere during the day. At night, the ionosphere undergoes changes due to the absence of direct sunlight, and the EEJ can be influenced by geomagnetic disturbances from solar storms or other space weather. Unlike during quiet periods, the behavior of the EEJ, particularly at night during extreme disturbances, has not been thoroughly studied. Utilizing high-precision MSS-1 measurements, we investigate the EEJ characteristics on both the dayside and nightside during a super geomagnetic storm. The daytime EEJ reacts differently during various storm phases, and the nighttime EEJ is sensitive to the onset of the storm. These findings indicate that the EEJ is significantly affected by extreme space weather events.

1. Introduction

The ionosphere is a region of Earth's upper atmosphere that is ionized by solar extreme ultraviolet (EUV) and X-ray radiation. It plays a crucial role in coupling between the ionosphere and the magnetosphere, affecting a wide range of geophysical phenomena, including ionospheric currents. Based on electron density, the ionosphere is divided into several layers, with the E-region being particularly significant for the formation and dynamics of ionospheric currents (Kelley, 2009).

The intensity of electric currents in the ionosphere is proportional to the content of charged particles. Zonal ionospheric currents are large-scale horizontal currents flowing east-west within the ionosphere, primarily driven by neutral winds, plasma pressure gradients, and electric fields, with significant variability across latitudes and local times (Alken et al., 2015). The equatorial electrojet (EEJ) dominates zonal currents near the magnetic equator, characterized by intense eastward or westward flow in the E-region. This phenomenon arises from the Cowling effect, in which the vertical Hall current is inhibited by boundary conditions, producing a vertical polarization electric field that drives an additional horizontal east–west current, thereby enhancing the effective (Cowling) conductivity (Cowling, 1932).

10.1029/2025JA034390

The daytime EEJ manifests as an eastward-flowing ionospheric current, driven principally by the dynamo electric field generated in the E-region. This dynamo mechanism arises from the interaction between atmospheric tidal winds–produced by solar thermal forcing and lunar gravitational effects–and Earth's magnetic field (Kelley, 2009). Predominantly, investigations into the daytime EEJ have focused on geomagnetically quiet conditions (Sripathi & Bhattacharyya, 2012; Zhang et al., 2022). The current system exhibits distinct diurnal and seasonal patterns, peaking between 10:00–14:00 local time and attaining maximum intensity during equinoxes when direct solar illumination optimizes ionospheric conductivity at equatorial latitudes (Yamazaki & Maute, 2017). The intensity and variability of EEJ are influenced not only by diurnal variations, seasonal changes, and solar cycle fluctuations but also by geomagnetic activity (Lei et al., 2018; Li et al., 2022; Yamazaki & Kosch, 2015).

The nighttime EEJ, especially during geomagnetic storms, is not well understood and differs significantly from daytime due to the lack of solar radiation. Satellite data, like CHAMP's, reveal a westward EEJ after 02:30 MLT, intensifying near sunrise, with enhanced currents over Africa and India (Zhou et al., 2020). Numerous studies have confirmed that the overshielding electric field can be generated not only by substorm activity but also during the convection reduction phase following the establishment of the shielding electric field due to enhanced magnetospheric convection (Fejer et al., 1979; Hashimoto et al., 2011; Kikuchi et al., 2003). During the expansion phase of substorms, the eastward overshielding field powers the night EEJ, enhancing positive bay phenomena, while substorm currents link to the equatorial ionosphere (Hashimoto et al., 2017). These currents demonstrate a strong westward flow in the evening-to-dawn sector, which is influenced by geomagnetic activity levels.

Previous studies have detailed the characteristics of zonal ionospheric currents and the electrojet perturbations under quiet conditions. However, the coupled response of the dayside and nightside to storm-time electric fields remains poorly understood. Spacecraft missions operating at low altitudes (∼430 km) and equipped with high-resolution measurement instruments are ideally suited for detailed investigations of the EEJ (Lühr et al., 2004). The Macau Scientific Satellite 1 (MSS-1) is the first Chinese satellite equipped with high-precision geomagnetic field measurement capabilities, orbiting at an altitude of approximately 450 km. The May 2024 Mother's Day geomagnetic storm is another G5-class storm following the Halloween geomagnetic storm in 2003. This research aims to analyze the dynamics of electrojet perturbations during this significant geomagnetic storm event, utilizing data from the MSS-1, thereby enhancing understanding of storm-time electrodynamics at low latitudes.

2. Data and Methods

2.1. Macau Scientific Satellite-1

The Macau Scientific Satellite-1, launched in February 2023 as the first satellite dedicated to geomagnetic observations in low-latitude regions, is a dual-satellite mission comprising spacecraft A and B. Spacecraft A (MSS-1A) operates in a near-circular orbit at an altitude of 450 km with an inclination of 41°, enabling its ascending node to process through all local times in approximately 53 days (Cheng et al., 2022). The satellite is equipped with an absolute scalar magnetometer, the Compact Digital Scalar Magnetometer (CDSM), alongside two vector magnetometers: the Fluxgate Magnetometer (FGM) and the Vector Field Magnetometer (VFM). In this study, we utilize the high-precision scalar magnetic field data acquired by the CDSM—sampling at 1 Hz—to investigate low-latitude magnetic field signatures during the geomagnetic storm from 10 May to 13 May 2024. During this storm, the MSS-1A satellite flew in sectors close to noon and midnight, and Swarm B also flew in these sectors with a separation of about 2 MLT. Their combined observations can therefore be used to obtain more detailed climatological information on the EEJ evolution.

2.2. Swarm Satellite Constellation

The European Space Agency (ESA) launched the Swarm mission on 22 November 2013 as a constellation of three identical satellites (Swarm-A, -B, and -C) to study the Earth's magnetic field (Friis-Christensen et al., 2006). Each satellite is equipped with an Absolute Scalar Magnetometer (ASM) for calibration and a VFM for vector measurements. In this study, we utilize data from Swarm B, which operates in a higher orbit (initial altitude of 511 km) at an inclination of 87.75°. Although Swarm B was initially orbiting approximately parallel to the lower A/C pair, the natural evolution of the orbit has altered this configuration over time. The EEJ magnetic signatures were determined using the Level 1b magnetic scalar products. With calibration models reducing scalar differences to generally below 0.5 nT (Tøffner-Clausen et al., 2016), Swarm B serves as a reliable reference for validating MSS-1A.

2.3. Correction of the Residual Magnetic Field

The method used to estimate the low-latitude magnetic field involves transforming scalar magnetic field data collected along the satellite's orbit into a set of line currents at E-region altitudes. Initially, the raw magnetic field measurements are corrected to subtract the influences from the Earth's core, crust, and magnetospheric fields using the CHAOS-7 geomagnetic field model, yielding a scalar residual, $F^{(1)}$. To extract the equatorial electrojet signature, the midlatitude Sq current contributions and any unmodeled external fields are removed for each orbit (Alken et al., 2013). The model, known as F_{Sq}, aims to capture the most precise magnetic signature of the EEJ.

Upon examining the magnetic field residuals during geomagnetic storms, it is essential to consider the residual effects of the ring current. The findings from this examination are summarized by the scalar residual F_{Dst}. We assumed a homogeneous external degree 1 field, corresponding to the lowest-order external spherical harmonic used as a first-order approximation of the global ring current effect, which supplements the Earth's dipole field. The total field residuals, ΔB, can be formulated as follows:

$$\Delta B = -\Delta RC\left(\frac{3\sin^2\beta - 1}{\sqrt{1+3\sin^2\beta}}\right),$$

where β is the dipole latitude. The values of ΔRC are determined by fitting Equation to the observed ΔB profiles (Lühr & Zhou, 2020). The magnetic effects generated by the ring current are completely represented by ΔB at $\beta = 0°$, and the ΔB signal disappears at $\pm 35.26°$ quasi-dipole latitude (QDlat) where $3\sin^2\beta - 1 = 0$.

2.4. Estimation of Current Density

In the following, we describe the procedure for deriving the latitudinal profiles of the current density from magnetic field measurements. By representing the current system as a series of east–west line currents parallel to lines of constant QD latitude, located at an altitude of 110 km and separated by 1° within the ±50° QD latitude, the height-integrated current density can be derived from the magnetic field component. According to Equation 2 in Lühr et al. (2004), the magnetic field perturbations at satellite altitude caused by an east–west line current can be written as

$$\begin{aligned} b_x &= -\frac{\mu_0}{2\pi}\frac{I\,h}{x^2+h^2}, \\ b_z &= \frac{\mu_0}{2\pi}\frac{I\,x}{x^2+h^2}. \end{aligned} \tag{1}$$

where b_x and b_z are the northward and downward components of the magnetic field, respectively, μ_0 is the permeability of free space, I is the line current strength of the eastward current, h is the height of the measurement point above the line current, and x is the northward displacement of the MSS-1A position from the current.

Based on Equation 1, for the ith satellite measurement point, the northward and downward magnetic field components generated by the jth line current can be expressed, following Zhou et al. (2020), as

$$\begin{aligned} b_x(i,j) &= -\frac{\mu_0}{2\pi}J(j)\,\Delta l\,\frac{h(i,j)}{x^2(i,j)+h^2(i,j)}, \\ b_z(i,j) &= \frac{\mu_0}{2\pi}J(j)\,\Delta l\,\frac{x(i,j)}{x^2(i,j)+h^2(i,j)}. \end{aligned} \tag{2}$$

where $J(j)$ is the height-integrated current density representing the jth line current, and Δl is the distance between adjacent line currents (here 110 km for 1° QDlat). With this formulation, two parameters are defined as $x(i,j) = R_{\mathrm{cur}}\sin(\Delta\beta(i,j))$ and $h(i,j) = R_{\mathrm{sat}} - R_{\mathrm{cur}}\cos(\Delta\beta(i,j))$, Here, $\Delta\beta(i,j)$ denotes the angular distance between the ith measurement point and the jth line current, R_{sat} is the radius of the satellite orbit, and R_{cur} denotes

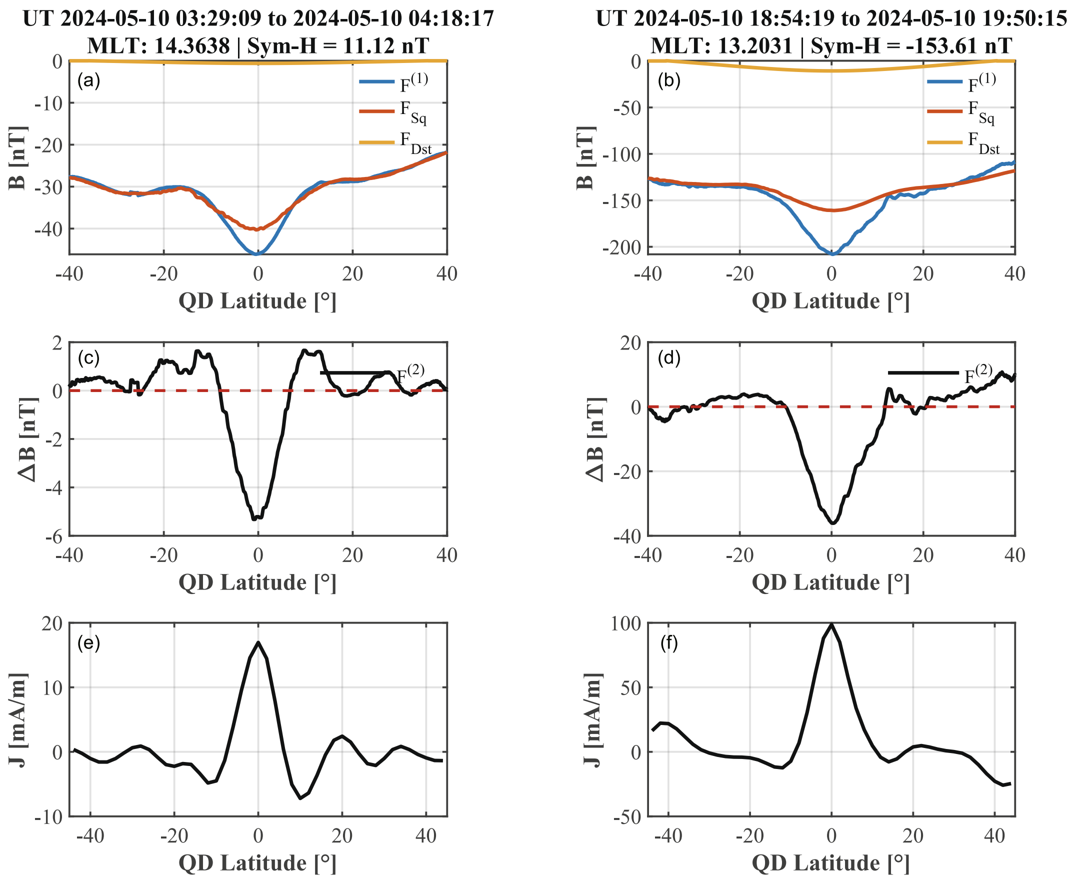

Figure 1. An example of the EEJ signals observed by MSS-1A during the geomagnetic storm, with the left side showing the period of magnetic quiet and the right side displaying the period of magnetic activity. (a) and (b): The scalar magnetic field residuals were calculated by subtracting the CHAOS.7 model (blue line). Internal and external spherical harmonic model fitted to mid-latitude data to filter out Sq and other effects (orange line). The residuals attributed to the ring current during the period of magnetic activity are shown in yellow. (c) and (d): The same profiles are displayed after subtracting the model, revealing the characteristic features of the EEJ. (e) and (f): Current density profiles derived by inverting magnetic field components.

the radius of the current layer center, which is assumed to be located at an altitude of 110 km above the Earth's surface.

Since the magnetic field contribution from the current, denoted by **b**, is much smaller than the unperturbed ambient field, represented by **B**, at satellite altitude, the scalar magnetic field perturbation of the current can be expressed, following Lühr et al. (2004), as

$$\Delta B = \frac{\mathbf{B} \cdot \mathbf{b}}{|\mathbf{B}|} = \frac{B_x b_x + B_z b_z}{|\mathbf{B}|}. \tag{3}$$

where B_x and B_z are the northward and downward components of the ambient magnetic field **B**, as derived from the CHAOS-7 model.

Figure 1 illustrates the latitude variation of the scalar magnetic field observed during the daytime by the MSS-1A satellite. The left side shows an example from a quiet magnetic period, while the right side displays an example from an active magnetic period. In Figures 1a and 1b, the blue line shows magnetic profile of the dayside $F^{(1)}$ residuals. The orange line represents modeled Sq currents, and the yellow line displays ring current effects during active magnetic periods. Figures 1c and 1d display the $F^{(2)}$ residuals obtained after subtracting the models from the same profile. A clear drop in the main magnetic field appears at the magnetic equator, caused by the EEJ. Our analysis methodology incorporates ring current corrections to isolate low-latitude current signatures. In this

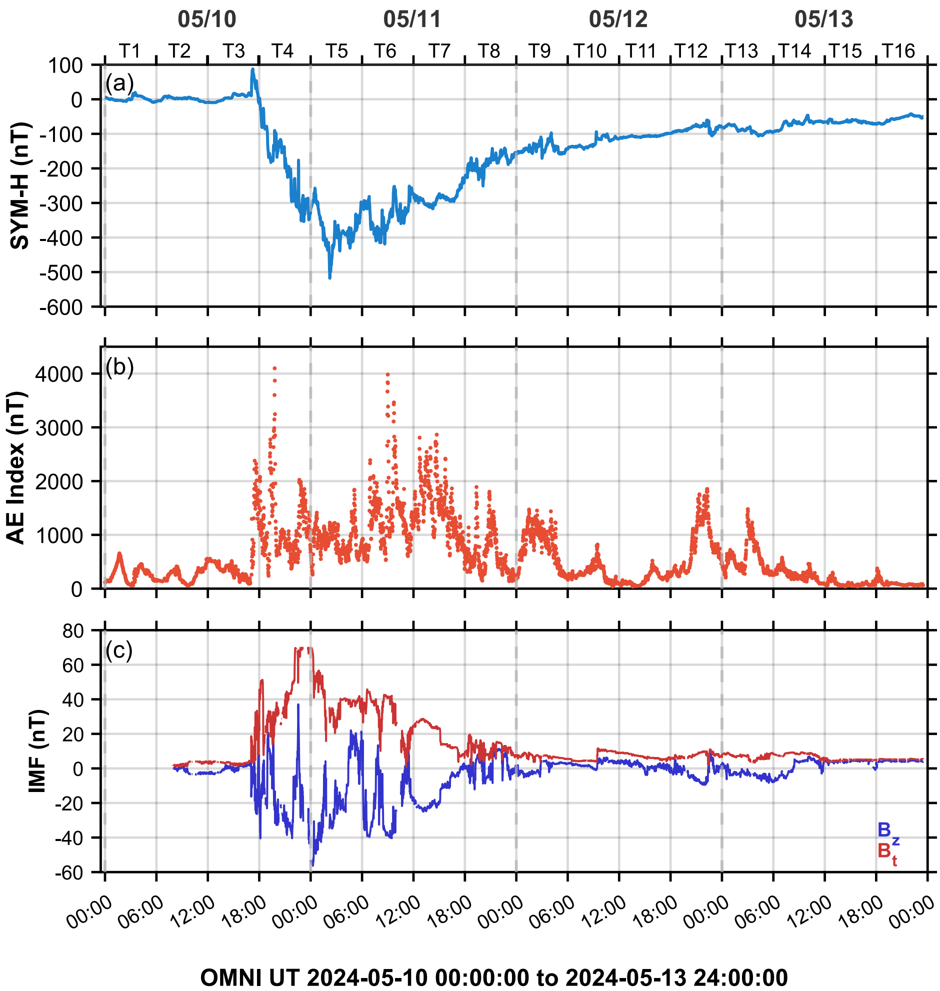

Figure 2. The geomagnetic storm conditions observed from 10 to 13 May 2024. Panels (a), (b), and (c) display the temporal variations of the SYM-H index, AE index, and IMF conditions, respectively.

manner, the correction for the residual magnetic field has been applied to satellite orbits during periods of magnetic disturbance. Assuming that the EEJ current flows at an altitude of 110 km, the derived current density is eastward and reaches a peak value of approximately 17 mA/m near the magnetic equator during the quiet period, as shown in Figure 1e. During the geomagnetically active event, the peak EEJ current density increases significantly to about 99 mA/m, as shown in Figure 1f.

3. Results and Discussion

3.1. Average Daytime Magnetic Field in Response to Geomagnetic Storm

Figure 2 shows the conditions of the geomagnetic storm that took place from May 10 to 13, 2024. The three panels, (a), (b), and (c) display the changes over time in the SYM-H index, the AE index, and the interplanetary magnetic field (IMF), respectively. The onset of the significant geomagnetic disturbance was initiated around 17:00 UT on May 10, coinciding with the southward turning of the IMF Bz component. The Super geomagnetic storm reached its minimum value of approximately −518 nT around 02:00 UT on May 11. Concurrently with the storm's onset, substorm occurred and continued until May 13, when the situation started to normalize. It is common for geomagnetic storms to be accompanied by substorms (Gonzalez et al., 1994), which tend to happen frequently during the main phase. The IMF components Bz and Btotal exhibited intricate fluctuations from the storm's onset until its gradual subsidence.

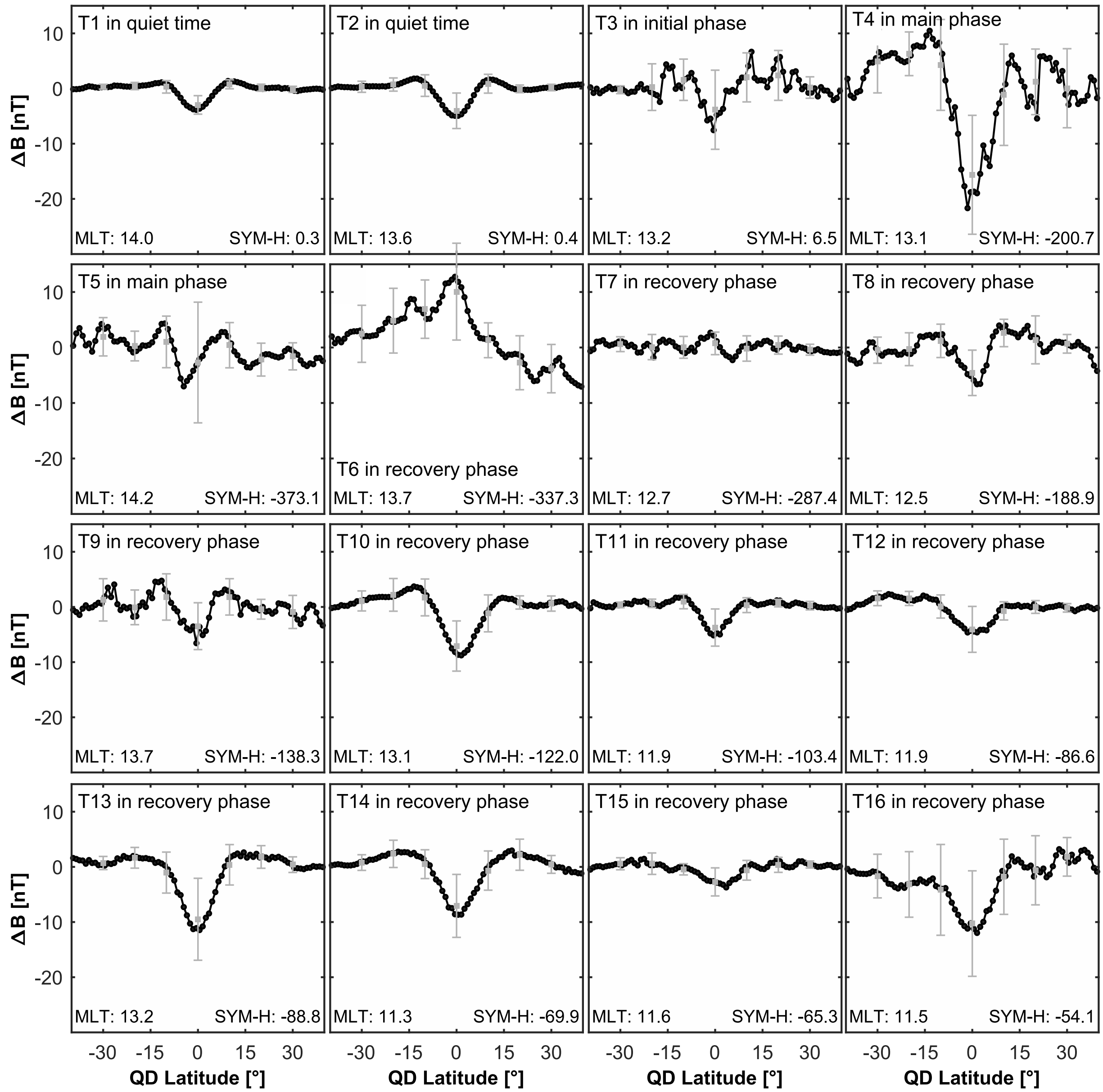

Figure 3. Dayside scalar residual magnetic field after subtracting contributions from the main field, crustal field, magnetospheric field, and Sq currents observed by MSS-1A during the 10–13 May 2024 geomagnetic storm. The solid curve depicts the average value for each latitude. Each subplot includes the average MLT and the average Dst index for reference.

The geomagnetic storm occurring from May 10 to 13, 2024, was divided into 16 intervals, labeled T_n (for $n = 1$, 2, …, 16), each encompassing a 6-hr duration. According to this segmentation, T_1 and T_2 denote the initial two 6-hr periods of geomagnetic quiet. T_3 designates storm onset. T_4 and T_5 correspond to the main phase of the storm. Subsequently, T_6 to T_{16} define the period of recovery from the geomagnetic storm. To assess the storm's effects, the changes in the magnetic field were categorized based on the Dst index, with each category representing a 6-hr span.

Figure 3 presents the dayside scalar residual magnetic field for each storm interval after removing contributions from the main geomagnetic field, crustal fields, magnetospheric currents, and Sq variations, as observed by MSS-1A. The solid curve represents the average value for each latitude. The dayside orbits have a mean magnetic local time (MLT) of approximately 13. During geomagnetic quiet time (T_1–T_2), the electrojet perturbation exhibited a predominantly eastward orientation. This orientation of electric currents produced a magnetic field at the satellite's altitude that contradicted the main geomagnetic field, resulting in negative residuals of around −7 nT near the magnetic equator. Concurrently, return currents were observed on either side of the ±10° quasi-dipole latitude band.

During the initial phase of the geomagnetic storm, the electrojet perturbations respond promptly and strongly. Nevertheless, because this phase is short-lived and the data is limited to a single satellite pass, there may be some uncertainties in the observed data. During the main phase of the storm (T_4–T_5), electrojet disturbances peak in intensity concurrent with the steep decline in the SYM-H index, exhibiting a drop of about −22 nT near the magnetic equator. Around 3 hours after the SYM-H index reaches its minimum value, the eastward electrojet perturbations strength persists but significantly weakens. During the transition from the main phase to the recovery phase (T_5–T_6), the enhanced high-latitude convection electric field leaks to low latitudes and affects the equatorial electrojet, likely due to changes in the penetration electric field from high latitudes (Yamazaki & Kosch, 2015).

During the recovery phase of the geomagnetic storm, the T_6 period reveals the distinctive features of the counter equatorial electrojet (CEJ), which align with a westward-directed equatorial electric field. This event is potentially linked to the shift in the IMF Bz component (C.-S. Huang, 2012). Following this phase, the eastward electrojet disturbance continues for roughly 60 hr, from intervals T_7 through T_{16}. The electrojet perturbations result in a decrease of approximately 8 nT near the dip equator, though this change is not observed on all satellite orbits. This prolonged disturbance, which primarily occurs during the recovery phase, is likely driven by the disturbance dynamo electric field that can persist for several hours after the cessation of high-latitude forcing (C.-M. Huang et al., 2005; Zaka et al., 2009). The "after-storm" effect, characterized by enduring disturbances during the recovery phase, typically persists for around 24 hr after the SYM-H index reaches its minimum. For long-lasting geomagnetic disturbances occurring after the first day of the recovery phase (T_{10}–T_{16}), persistent cases exhibit pronounced dayside eastward EEJ, indicating enhanced eastward electric fields and an intensified equatorial fountain (Li et al., 2022). This persistent enhancement generally results in the intensification of the equatorial ionization anomaly. However, it should also be considered that a steady-state penetration electric field, which weakens gradually throughout the recovery phase, may still play a role. We believe that during magnetic storms (i.e., T_3–T_{16}), the observed phenomena are affected to varying degrees by both prompt penetration electric fields and disturbance dynamo electric fields processes, although it remains challenging to separate their respective contributions.

Figure 4 presents the dayside scalar residual magnetic field observed by Swarm B at an altitude of approximately 506 km and around 11 MLT, during the 10–13 May 2024 geomagnetic storm. Contributions from the main field, crustal field, magnetospheric field, and Sq currents have been subtracted. Following the storm onset, the eastward electrojet perturbations responded significantly, peaking at approximately −10 nT near the magnetic equator during the main phase (T_4) . During the T_5 to T_6 interval, a pronounced CEJ was observed, corresponding to the T6 interval in MSS-1A and attributed to the turning of the IMF Bz component. In the subsequent recovery phase, the EEJ stabilized at around −5 nT, consistent with quiet-time climatology. Overall, the dayside EEJ evolution observed by Swarm B during the storm closely resembles that derived from MSS-1A.

Understanding the general patterns of daytime ΔB variations, we observed EEJ signals across different levels of magnetic disturbance. To estimate these, we primarily adhere to the methodology employed by Zhou et al. (2020), aiming to invert the current density from magnetic field profile. The detailed calculation method is described in Section 2.3. Figure 5 presents the average characteristics of the typical EEJ signal under various magnetic disturbance conditions. From left to right, the figure depicts the following periods: the quiet time before the magnetic storm (T_1–T_2), the initial and main phases of the magnetic storm when disturbances are more intense (T_3–T_5), and the recovery phase of the magnetic storm (T_6–T_{16}). The results indicate a clear relationship between the intensity of a magnetic storm and its impact on the daytime EEJ.

As storm intensity increases, the disturbances in the daytime dominant eastward EEJ become more obvious, and the current density increases accordingly. Prior to the magnetic storm, the minimum EEJ value appears at the magnetic equator, reaching as low as −4.2 nT, with a corresponding current density of up to 13.6 mA/m. During major magnetic storm events, the penetration of eastward electric fields induced by southward IMF Bz component results in extreme intensification of the EEJ. The EEJ generated at low latitudes can reach a minimum value close to the magnetic equator of −20.8 nT, with a corresponding current density of 75.2 mA/m. The "after-storm" effect, which is evident during the recovery phase as shown in Figure 5c, persists even after the geomagnetic

10.1029/2025JA034390

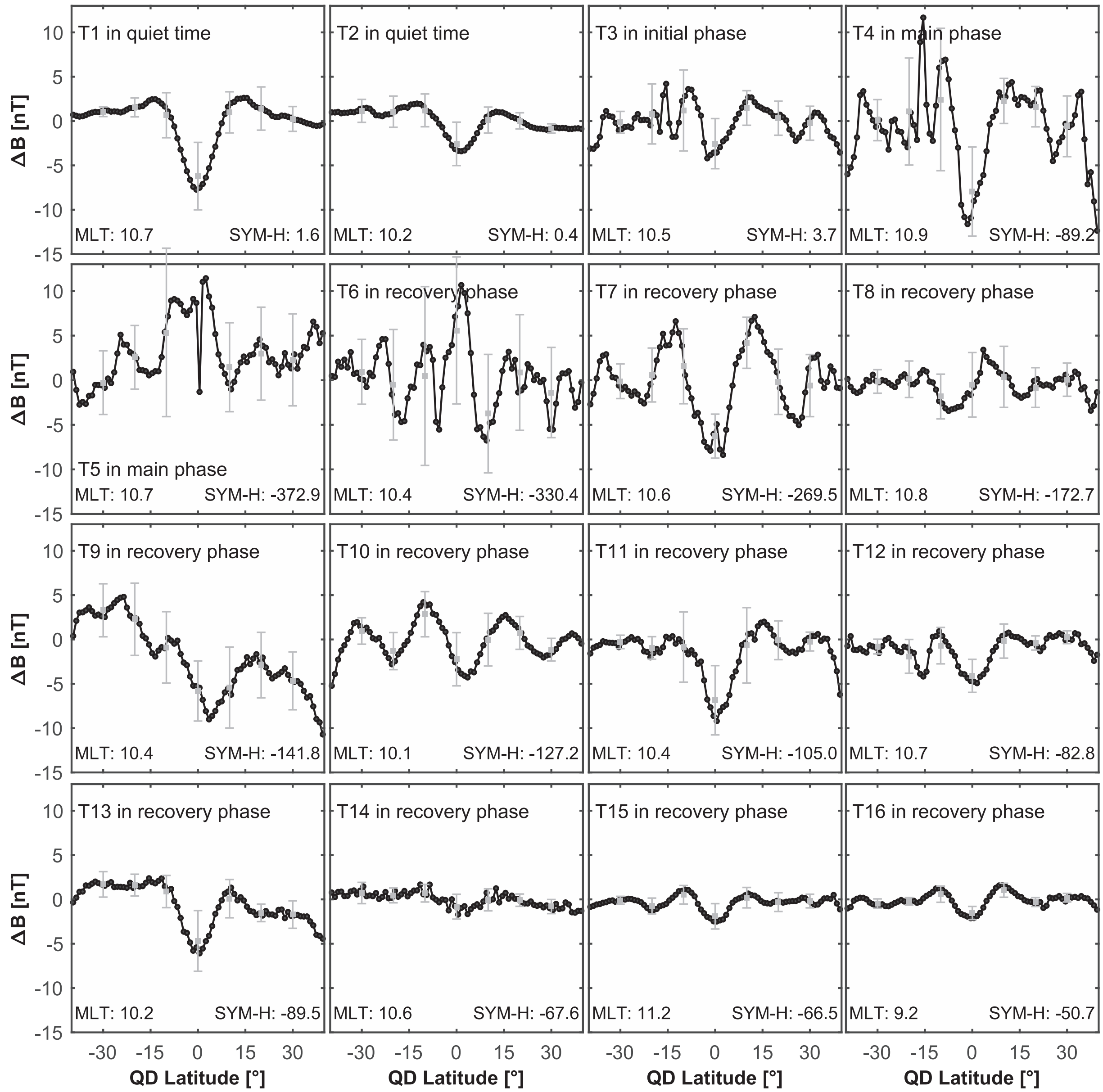

Figure 4. Similar to Figure 3, but presenting the dayside scalar residual magnetic field as observed by Swarm B.

activity has subsided (Blanc & Richmond, 1980; C.-M. Huang et al., 2005; Yamazaki & Kosch, 2015). During the recovery phase, the EEJ at low latitudes near the magnetic equator reaches a minimum value of −8.3 nT, with a corresponding current density of 25 mA/m.

Satellite observations have demonstrated a strong correlation between the dayside EEJ and geomagnetic disturbances (Alken et al., 2015; Li et al., 2022; Yamazaki & Kosch, 2015). During this super geomagnetic storm, the southward turning of IMF Bz component led to an enhancement of the magnetospheric penetration electric field, which in turn intensified the equatorial eastward electric field during the daytime, significantly strengthening the EEJ. The increased particle precipitation and the injection of more energy into the high-latitude upper atmosphere resulted in stronger and more persistent disturbed winds, generating a disturbed dynamo electric field. This sustained activity also influenced the EEJ during the recovery phase of the storm. We suggest that during the main phase of the storm, the dayside EEJ intensity increased by 5 times due to penetrating electric fields, while disturbance dynamo effects restored the current levels to normal during the recovery phase.

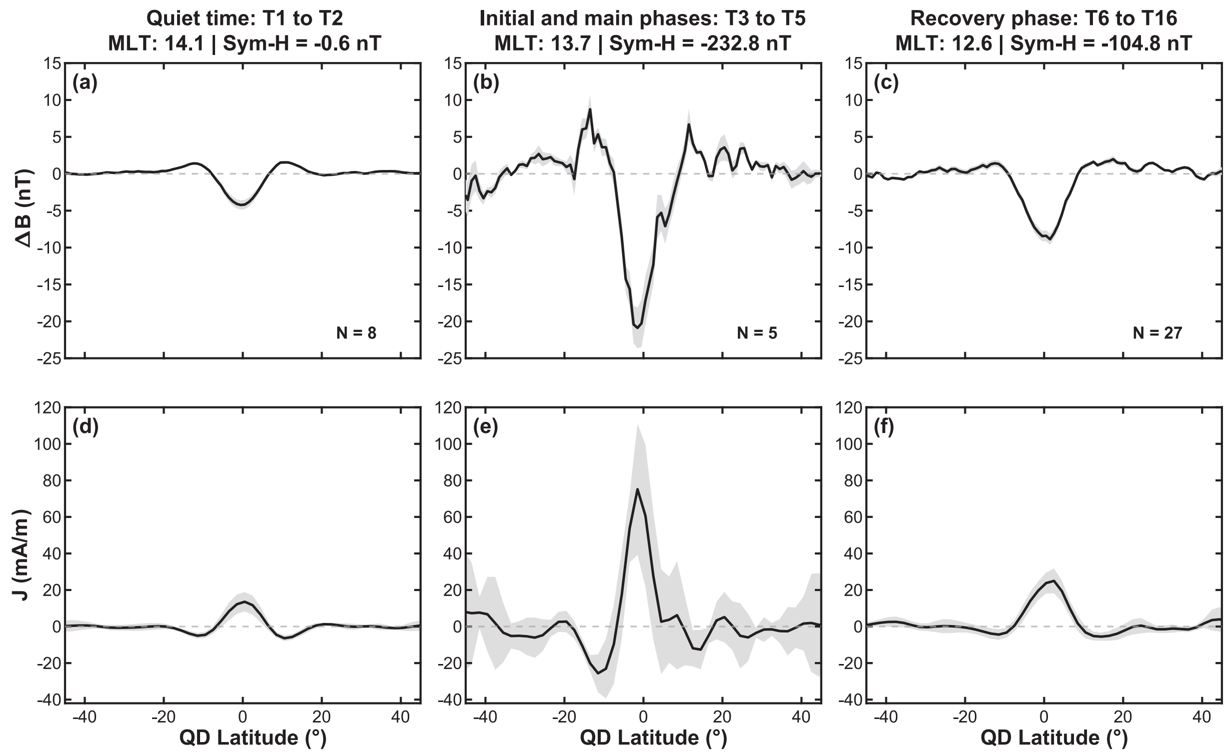

Figure 5. Average characteristics of the EEJ under different magnetic disturbance conditions, including (left) quiet time (T1–T2), (middle) the initial and main phases (T3–T5), and (right) recovery phase (T6–T16). The top and bottom panels, respectively, depict the variations of the average EEJ signal and the average current density profiles. Each subplot also displays the average MLT and the average Dst index.

3.2. Average Nighttime Magnetic Field in Response to Geomagnetic Storm

While the daytime dynamics of the electrojet are well-documented, its behavior at night is less clear. Previous research has provided some insights into the nighttime equatorial electrojet, but the number of studies are limited (Abdu et al., 2007; Shinbori et al., 2013; Zhou et al., 2020). Another focus of this paper is to examine the features of electrojet disturbances during geomagnetic storms at night, using data from the MSS-1 satellite.

Figure 6 presents an analysis of the residual magnetic fields in the nightside sector adjacent to the magnetic equator during the geomagnetic storm of 10–13 May 2024, as observed by MSS-1A. The data processing methodology for this figure is in line with that used for Figure 3. Each subplot is accompanied by the average MLT and the average Dst index for reference. The results indicate that electrojet perturbations on the nightside undergo significant disturbances during geomagnetic storm periods, such as those identified during phases T_3–T_8, in contrast to the quiet magnetic periods (T_1–T_2). Although nightside EEJ signals are generally weak and the number of available satellite orbits is limited, pronounced low-latitude electrojet perturbations are evident during these periods, accompanied by intensified substorm activity associated with the geomagnetic storm. Figure 7 shows the evolution of the nightside EEJ from Swarm B, derived using the same method. Strong electrojet perturbations were observed during the intervals T_3–T_8, which coincided with frequent storm activity.

Subsequently, we investigated the characteristics of the magnetic field to infer the height-integrated current density of the zonal ionospheric currents in the nighttime low to mid-latitude regions. Figure 8 shows two typical behaviors that may represent the nighttime EEJ under different magnetic disturbance conditions. Given the substantial differences between nighttime and daytime ionospheric conditions, and the expectation that nighttime ionospheric currents at middle and low latitudes predominantly flow near the F region, three representative current heights (110, 230, and 300 km) were tested in Figures 8e and 8f (Zhou & Luehr, 2023). The results indicate that the assumed current height has only a minor influence on the derived current profiles, although higher assumed heights tend to slightly underestimate the EEJ intensity.

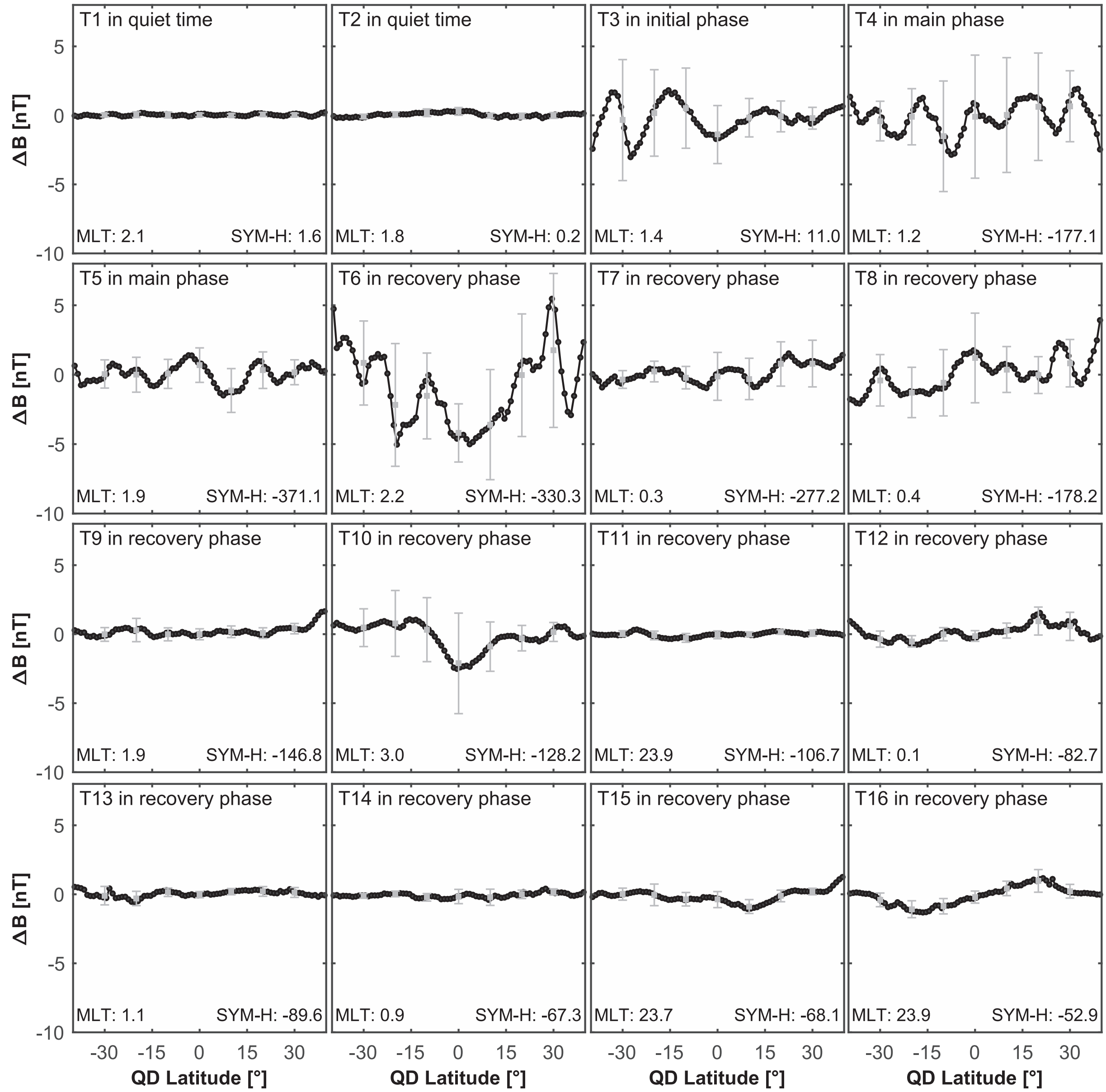

Figure 6. Nightside scalar residual magnetic field after subtracting contributions from the main field, crustal field, magnetospheric field, and Sq currents observed by MSS-1A during the 10–13 May 2024 geomagnetic storm. The solid curve depicts the average value for each latitude. Each subplot includes the average MLT and the average Dst index for reference.

The left panels of Figure 8 present a nighttime mid-latitude case of a strong eastward current jet, with a peak current density of about 35 mA/m (Figure 8e) and a corresponding magnetic perturbation of approximately −12 nT (Figure 8c). This feature is observed in the midnight sector at about 16° QDlat during the recovery phase, when SYM-H reached −367.8 nT. At the same time, a pronounced westward current jet was observed near the equator in the noon sector (Figure 3, T6). This temporal coincidence suggests a possible connection between these two phenomena. Considering that the generation mechanism of the CEJ involves westward neutral winds, we suggest that disturbance driven neutral winds may contribute to the enhanced eastward current jets observed at middle latitudes (Xiong et al., 2025). In this super geomagnetic storm, strong eastward current jets at middle latitudes are more frequently observed during the early recovery phase, a behavior that has been only sparsely documented in previous studies and therefore deserves further investigation.

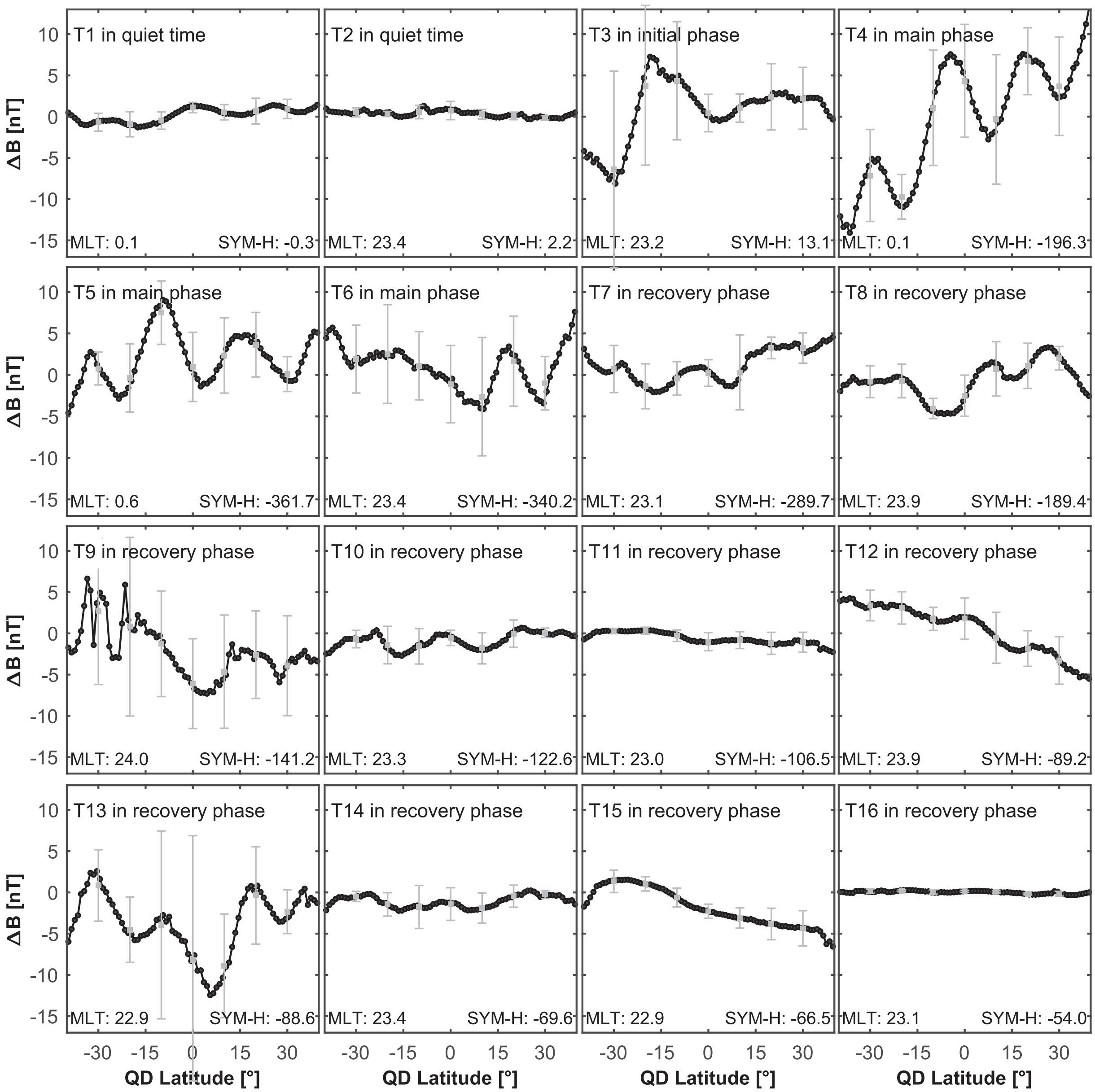

Figure 7. Similar to Figure 6, but presenting the nightside scalar residual magnetic field as observed by Swarm B.

The right panels of Figure 8 show a nighttime westward current jet near the equator, with a peak current density of −7.8 mA/m (Figure 8f) and a corresponding magnetic perturbation of about 2.4 nT (Figure 8d). This signal typically flows westward and intensifies with increasing storm activity, which is consistent with the direction of the large electric field present at night (Fejer, 2011). In the low-latitude region, an eastward ionospheric F-region current is commonly observed after sunset. As it gets closer to midnight, this current almost disappears and then shifts direction from eastward to westward. This westward current at low latitudes becomes stronger at dawn (Zhou et al., 2020). Our observations, which focus on the time around midnight, have detected a westward current near the magnetic equator. Given that individual events in our study only cover the period around midnight, we are not able to capture the more intense current that occurs at dawn. The features of these nightside electrojet disturbances are more obvious under magnetic disturbance conditions and might be linked to the impact of prompt penetrating electric fields or the disturbance dynamo electric field, as discussed by Abdu et al. (2007). The overshielding electric field, a consequence of substorm activity and the reduction in convection following the development of the shielding electric field due to enhanced magnetospheric convection (Gonzalez et al., 1994;

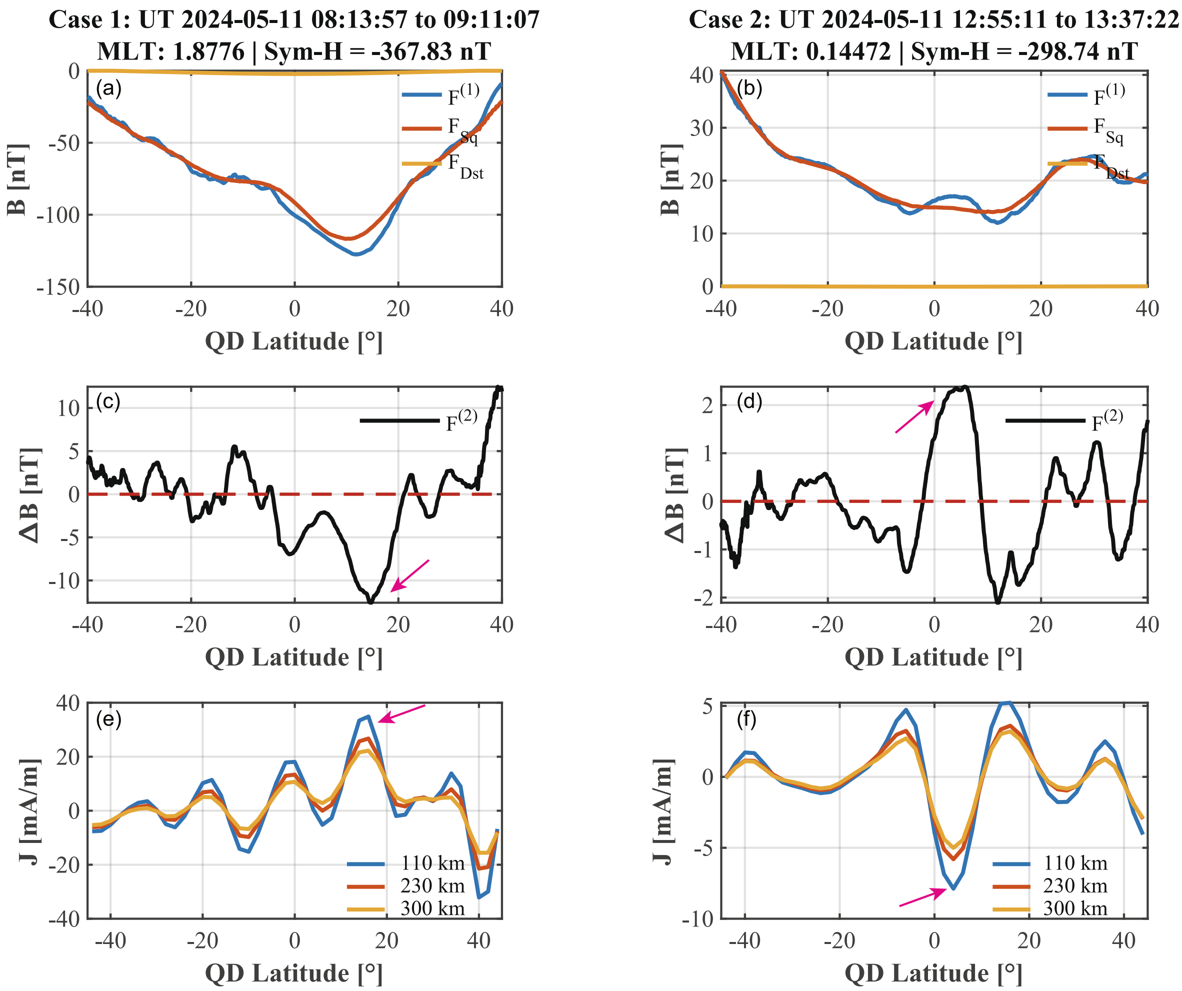

Figure 8. Two types of nighttime current jet signatures observed on 11 May 2024. Left panel: A strong eastward current jet observed at middle latitudes. Right panel: A westward current jet observed near the magnetic equator.

Hashimoto et al., 2011; Wei et al., 2009) also contributes to the generation of the EEJ on the nightside. Hashimoto et al. (2017) suggest that the overshielding electric field is generated at the onset of the substorm, often followed by another overshielding event during the recovery phase, leading to a two-step development. In our study, this two-step overshielding is reflected in (a) the initial overshielding at substorm onset (i.e., T_3–T_4) and (b) the subsequent overshielding associated with the northward turning of the IMF Bz (i.e., T_5–T_{10}), which corresponds to the substorm recovery phase due to convection reduction. The onset-triggered overshielding is caused by the intensification of Region 2 field-aligned currents due to magnetotail dipolarization, while the second overshielding is attributed to convection reduction following a northward turning of the IMF. Unlike the strong eastward current observed during the dayside, the weak westward current at night exhibits more complex behavior. We believe this complexity is related to changes in the electric field caused by intense magnetic disturbances.

4. Conclusions

Utilizing high-precision magnetic field measurements from the MSS-1A satellite together with observations from Swarm B, this study investigates the characteristics of the EEJ on both the dayside and nightside during a super geomagnetic storm on 10–13 May 2024. The key findings of the research can be summarized as follows:

1. During the storm, the dayside EEJ predominantly flows eastward, showing a more intense response in the initial and main phases than during quiet times as revealed by combined MSS-1A and Swarm B observations

in the noon sector. Near the magnetic equator, the EEJ reaches −20.8 nT, corresponding to a current density of 75.2 mA/m. In the recovery phase, the disturbed electrodynamic field persists, with the EEJ at low latitudes attaining −8.3 nT and a current density of 25 mA/m, resembling the stable patterns of quiet periods.
2. On the nightside, electrojet disturbances are generally weaker; however, based on combined MSS-1A and Swarm B observations in the midnight sector, they become significantly enhanced during periods of intense storm activity. In the midnight sector, one case shows a strong eastward current jet at low to middle latitudes, while another exhibits a westward current jet near the equator, corresponding to periods when the dayside EEJ in the noon sector is significantly enhanced or even reversed.
3. The enhancement of the dayside EEJ and the emergence of the nightside EEJ are highly sensitive to the onset of the geomagnetic storm. The storm onset can substantially modify the ionospheric electrical conductivity and associated current systems, leading to pronounced intensification on the dayside and the development of EEJ signatures on the nightside.

Conflict of Interest

The authors declare no conflicts of interest relevant to this study.

Availability Statement

The OMNI data set is available from the OMNIWeb service online of NASA/GSFC's Space Physics Data Facility (https://spdf.gsfc.nasa.gov/pub/data/omni/). Macao Foundation (MF) and China National Space Administration (CNSA) provided MSS-1 satellite data is gratefully acknowledged (https://mss.must.edu.mo/datadownload.html). We gratefully acknowledge the European Space Agency (ESA) for providing the Swarm data, which can be accessed at https://swarm-diss.eo.esa.int/.

Acknowledgments
Thanks to the China National Space Administration and the Macau Foundation for their support. We wish to thank all personnel at DFH, DTU, IWF, NSSC, and MUST for their contributions to satellite launch and data processing. This work is supported by the National Natural Science Foundation of China (NSFC) under Grants 42241112 and 42441805, the Science and Technology Development Fund, Macau SAR (File No. 0008/2024/AKP), the MUST General Research Grant (No. FRG-24-047-SSI), and by the Specialized Research Fund for State Key Laboratories.

References

Abdu, M. A., Maruyama, T., Batista, I. S., Saito, S., & Nakamura, M. (2007). Ionospheric responses to the October 2003 superstorm: Longitude/local time effects over equatorial low and middle latitudes. *Journal of Geophysical Research*, *112*(A10). https://doi.org/10.1029/2006ja012228

Alken, P., Maus, S., Chulliat, A., Vigneron, P., Sirol, O., & Hulot, G. (2015). Swarm equatorial electric field chain: First results. *Geophysical Research Letters*, *42*(3), 673–680. https://doi.org/10.1002/2014gl062658

Alken, P., Maus, S., Vigneron, P., Sirol, O., & Hulot, G. (2013). Swarm scarf equatorial electric field inversion chain. *Earth Planets and Space*, *65*(11), 1309–1317. https://doi.org/10.5047/eps.2013.09.008

Blanc, M., & Richmond, A. (1980). The ionospheric disturbance dynamo. *Journal of Geophysical Research*, *85*(A4), 1669–1686. https://doi.org/10.1029/ja085ia04p01669

Cheng, Z., Tang, K., Zhang, Z., Zhang, H., Li, P., & Long, M. (2022). Design and analysis of the Macau science satellite-1’s laser retro-reflector array. *Earth and Planetary Physics*, *7*(1), 131–135. https://doi.org/10.26464/epp2023008

Cowling, T. (1932). Magnetism, solar: The electrical conductivity of an ionised gas in the presence of a magnetic field. *Monthly Notices of the Royal Astronomical Society*, *93*(1), 90–97. https://doi.org/10.1093/mnras/93.1.90

Fejer, B. G. (2011). Low latitude ionospheric electrodynamics. *Space Science Reviews*, *158*(1), 145–166. https://doi.org/10.1007/s11214-010-9690-7

Fejer, B. G., Gonzales, C., Farley, D., Kelley, M., & Woodman, R. (1979). Equatorial electric fields during magnetically disturbed conditions 1. The effect of the interplanetary magnetic field. *Journal of Geophysical Research*, *84*(A10), 5797–5802. https://doi.org/10.1029/ja084ia10p05797

Friis-Christensen, E., Lühr, H., & Hulot, G. (2006). Swarm: A constellation to study the earth’s magnetic field. *Earth Planets and Space*, *58*(4), 351–358. https://doi.org/10.1186/bf03351933

Gonzalez, W., Joselyn, J.-A., Kamide, Y., Kroehl, H. W., Rostoker, G., Tsurutani, B. T., & Vasyliunas, V. (1994). What is a geomagnetic storm? *Journal of Geophysical Research*, *99*(A4), 5771–5792. https://doi.org/10.1029/93ja02867

Hashimoto, K., Kikuchi, T., Tomizawa, I., & Nagatsuma, T. (2017). Substorm overshielding electric field at low latitude on the nightside as observed by the hf doppler sounder and magnetometers. *Journal of Geophysical Research: Space Physics*, *122*(10), 10–851. https://doi.org/10.1002/2017ja024329

Hashimoto, K., Kikuchi, T., Watari, S., & Abdu, M. (2011). Polar-equatorial ionospheric currents driven by the region 2 field-aligned currents at the onset of substorms. *Journal of Geophysical Research*, *116*(A9). https://doi.org/10.1029/2011ja016442

Huang, C.-M., Richmond, A., & Chen, M.-Q. (2005). Theoretical effects of geomagnetic activity on low-latitude ionospheric electric fields. *Journal of Geophysical Research*, *110*(A5). https://doi.org/10.1029/2004ja010994

Huang, C.-S. (2012). Statistical analysis of dayside equatorial ionospheric electric fields and electrojet currents produced by magnetospheric substorms during sawtooth events. *Journal of Geophysical Research*, *117*(A2). https://doi.org/10.1029/2011ja017398

Kelley, M. C. (2009). *The earth’s ionosphere: Plasma physics and electrodynamics* (Vol. 96). Academic Press.

Kikuchi, T., Hashimoto, K., Kitamura, T.-I., Tachihara, H., & Fejer, B. (2003). Equatorial counter electrojets during substorms. *Journal of Geophysical Research*, *108*(A11). https://doi.org/10.1029/2003ja009915

Lei, J., Huang, F., Chen, X., Zhong, J., Ren, D., Wang, W., et al. (2018). Was magnetic storm the only driver of the long-duration enhancements of daytime total electron content in the Asian-Australian sector between 7 and 12 September 2017? *Journal of Geophysical Research: Space Physics*, *123*(4), 3217–3232. https://doi.org/10.1029/2017ja025166

Li, Q., Zhang, R., Liu, L., Kuai, J., Yang, N., Zhong, J., et al. (2022). Persistent eastward eej enhancement during the geomagnetic storm recovery phases. *Journal of Geophysical Research: Space Physics*, *127*(5), e2022JA030258. https://doi.org/10.1029/2022ja030258

Lühr, H., Maus, S., & Rother, M. (2004). Noon-time equatorial electrojet: Its spatial features as determined by the champ satellite. *Journal of Geophysical Research*, *109*(A1). https://doi.org/10.1029/2002ja009656

Lühr, H., & Zhou, Y.-L. (2020). Residuals to the chaos-6 geomagnetic field model caused by magnetospheric currents during enhanced magnetic activity. *Geochemistry, Geophysics, Geosystems*, *21*(6), e2020GC008976. https://doi.org/10.1029/2020gc008976

Shinbori, A., Hori, T., Tanaka, Y., Koyama, Y., Kikuchi, T., & Nagatsuma, T. (2013). Global distributions of storm-time ionospheric currents as seen in geomagnetic field variations. *Advances in Polar Sciences*, *24*(4), 296–314.

Sripathi, S., & Bhattacharyya, A. (2012). Quiet time variability of the gps tec and eej strength over Indian region associated with major sudden stratospheric warming events during 2005/2006. *Journal of Geophysical Research*, *117*(A5). https://doi.org/10.1029/2011ja017103

Tøffner-Clausen, L., Lesur, V., Olsen, N., & Finlay, C. C. (2016). In-flight scalar calibration and characterisation of the swarm magnetometry package. *Earth Planets and Space*, *68*(1), 129. https://doi.org/10.1186/s40623-016-0501-6

Wei, Y., Pu, Z., Hong, M., Zong, Q., Ren, Z., Fu, S., et al. (2009). Westward ionospheric electric field perturbations on the dayside associated with substorm processes. *Journal of Geophysical Research*, *114*(A12). https://doi.org/10.1029/2009ja014445

Xiong, C., Huang, Y., Wang, F., Lühr, H., Zhou, Y., & Zhu, J. (2025). Responses of the ionospheric zonal currents from equator to middle latitudes during the intense geomagnetic storm on 10–12 May 2024. *Journal of Geophysical Research: Space Physics*, *130*(7), e2025JA033992. https://doi.org/10.1029/2025ja033992

Yamazaki, Y., & Kosch, M. J. (2015). The equatorial electrojet during geomagnetic storms and substorms. *Journal of Geophysical Research: Space Physics*, *120*(3), 2276–2287. https://doi.org/10.1002/2014ja020773

Yamazaki, Y., & Maute, A. (2017). Sq and eej—A review on the daily variation of the geomagnetic field caused by ionospheric dynamo currents. *Space Science Reviews*, *206*(1), 299–405. https://doi.org/10.1007/s11214-016-0282-z

Zaka, K., Kobea, A., Assamoi, P., Obrou, O., Doumbia, V., Boka, K., et al. (2009). Latitudinal profile of the ionospheric disturbance dynamo magnetic signature: Comparison with the dp2 magnetic disturbance. *Annales Geophysicae*, *27*(9), 3523–3536. https://doi.org/10.5194/angeo-27-3523-2009

Zhang, K., Wang, H., & Wang, W. (2022). Local time variations of the equatorial electrojet in simultaneous response to subauroral polarization streams during quiet time. *Geophysical Research Letters*, *49*(7), e2022GL098623. https://doi.org/10.1029/2022gl098623

Zhou, Y.-L., & Luehr, H. (2023). Average ionospheric mid-and low-latitude currents from e-and f-region altitudes, derived by the swarm constellation. *Journal of Geophysical Research: Space Physics*, *128*(6), e2022JA031234. https://doi.org/10.1029/2022ja031234

Zhou, Y.-L., Lühr, H., & Alken, P. (2020). Average ionospheric middle and low latitudes nighttime zonal currents deduced from champ. *Journal of Geophysical Research: Space Physics*, *125*(8), e2019JA027702. https://doi.org/10.1029/2019ja027702